Bayesian Inference of Task-Based Functional Brain Connectivity Using Markov Chain Monte Carlo Methods

M Faizan Ahmad, James Murphy, Deniz Vatansever, Emmanuel A Stamatakis and Simon J Godsill

***Abstract*—The study of functional networks in the brain is essential in order to gain a better insight into its diverse set of operations and to characterise the associated normal and abnormal behaviours. Present methods of analysing fMRI data to obtain functional connectivity are largely limited to approaches such as correlation, regression and independent component analysis, which give simple point estimates. By contrast, we propose a stochastic linear model in a Bayesian setting and employ Markov Chain Monte Carlo methods to approximate posterior distributions of full connectivity and covariance matrices. Through the use of a Bayesian probabilistic framework, distributional estimates of the linkage strengths are obtained as opposed to point estimates, and the uncertainty of the existence of such links is accounted for. We decompose the connectivity matrix as the Hadamard product of binary indicators and real-valued variables, and formulate an efficient joint-sampling scheme to infer them. The well-characterised somato-motor network is examined in a self-paced, right-handed finger opposition task based experiment, while nodes from the visual network are used for contrast during the same experiment. Unlike for the visual network, significant changes in connectivity are found in the motor network during the task. Our work provides a distributional metric for functional connectivity along with causality information, and contributes to the collection of network level descriptors of brain functions.**

***Index Terms*—functional connectivity, BOLD, DCM, Gibbs sampling**

I. Introduction

RECENT research in the field of neuroimaging has discovered the significance of quantifying and tracking the dynamic aspects of functional networks in order to obtain a thorough description of the brain and to gain a better insight into the mechanisms behind its several operations. Through the notion of functional connectivity of BOLD (blood oxygenation level dependent) data collected during fMRI scanning, the brain has been functionally subdivided into distinct large-scale networks (LSNs) by identifying the statistical interdependences of signals from remote brain regions. LSNs with associative connections such as fronto-parietal, default mode, dorsal and ventral attention, as well as primary somato-sensory networks belonging to the visual, auditory and motor domains, have all been identified not only during task execution [1], but also during no-task resting state [2]. Though there is still much speculation in the sphere of cognitive neuroscience about the applicability and usefulness of such temporal connections amongst spontaneous BOLD signals, these networks have been shown to be robust and reproducible [3] [4]. Remarkable overlap has been observed with not only known spatial activation maps from investigations on the neural correlates of cognitive processing [5] [6], but also with the underlying structural connectivity [7] [8].

The most commonly used metrics to determine functional connectivity involve pairwise correlation and mutual information between time series obtained from pre-defined regions of interest (ROIs), thus indicating quantifiable relationships amongst distant brain regions without signifying causal interactions [9] [10] [11] [12] [13]. For example, one typical univariate method termed seed-based functional connectivity is used to detect relationships between an ROI and the rest of the brain, whereas multivariate approaches such as independent component analysis (ICA) find a number of temporally correlated components with maximal spatial independence [14] [15] [16] [17]. These methods have provided tremendous utility in characterising not only normal brain functions, but also alterations in brain connectivity architecture and LSN interactions in neuropsychiatric disorders such as schizophrenia [18], traumatic brain injury [19] [20] [21] as well as in normal ageing [22] and under propofol-induced sedation [23].

Though simple to use and easily scalable to large sized networks, these methods provide simple point estimates which do not incorporate uncertainty into their computations and are sensitive to the experimental characteristics of the data used. We introduce a more sophisticated approach of inferring functional connectivity by employing Markov Chain Monte Carlo (MCMC) methods within a Bayesian framework, which sets the problem in distributional terms and accounts for experimental error as well as the uncertainty on prior assumptions. As opposed to point estimates, entire posterior distributions of the unknown parameters are sought. Because it is not possible to correctly deduce the form of unknown

M F Ahmad* (mfa37@cam.ac.uk), J Murphy (jm362@cam.ac.uk) and S J Godsilll (sjg@eng.cam.ac.uk) are affiliated with the Signal Processing Group, Department of Engineering, University of Cambridge, Trumpington St, Cambridge CB2 1PZ, UK

D Vatansever (ddsv2@cam.ac.uk) and E A Stamatakis (eas46@cam.ac.uk) are affiliated with the Division of Anaesthesia, Department of Clinical Neurosciences, Addenbrooke's Hospital, Hills Road, Cambridge CB2 0QQ, UK.

system matrices (both connectivity and noise) in terms of a small number of scalar parameters using knowledge of any underlying physical systems, full matrices in a linear state space model could be inferred along with the additional benefit of providing causal inference.

Our state-space approach is akin to the models described in the wide literature on Dynamic Causal Modelling (DCM) [24] [25] [26] [27] and Structural Equation Modelling (SEM) [28] [29], which are used to describe directional coupling among brain regions at the neuronal state level; however, we avail a similar connectivity framework for dependences among BOLD signals directly instead. The concept of predictability indicating influence in the MVAR model matches that used in Granger causality [30] [31] [32], and the state transition equation could also be seen similar to the General Linear Model (GLM) [33] [34] [35], though here connectivity is sought among fMRI data directly as opposed to any design matrices.

In the context of these models, much work has been done to infer interactions at the neuronal state level, widely known as effective connectivity, using Bayesian approaches [36] [37] [38] [39]. However, the use of such methods to find functional connectivity among BOLD signals is limited. Most notably, a Bayesian approach has been employed in [40] by inferring posteriors of partial correlations, but this does not provide any information about causality as in our proposed method. In [41], the posteriors of regression coefficients are sought but through a pairwise approach, in contrast to a full system inference. Additionally, [42] [43] use Bayesian frameworks for regularisation schemes to introduce sparsity in functional networks.

We apply our methodology to fMRI data from a finger opposition paradigm with task and fixation conditions investigating dynamics of the well-characterised somato-motor network, while using the visual network as a control case. We hypothesised that given the previously observed changes in somato-motor network connectivity with motor skill acquisition [7] [44], our methodology would reflect dynamic differences in the interactions of the motor network regions, which would not be present in the visual network.

This paper consists of five sections. The model is described in Section II in terms of the state and observation equations and the associated probability distributions. This is followed by the explanation of the Gibbs sampler in order to infer functional connectivity in different task conditions. The algorithm is first tested on instances of synthetic data in Section III before it is applied to real life cases in Section IV. Conclusions and suggestions for future work are discussed in Section V.

II. Methods

The use of Bayesian methods results in consistent estimates of the system quantities as well as of any functions of these parameters. Analogous to the concept of thresholding in conventional methods, we incorporate a sparse representation a priori by suitable re-parameterisation of the model [45] [46]. Not only does it provide a more representative description through a smaller number of significant parameters, but it also yields more efficient results and requires less storage. In addition, the use of conjugate priors requires less algorithm tuning and achieves even further improvement in efficiency [47].

A linear state space model is defined as:

$$X_t = AX_{t-1} + W_t, \tag{1}$$

where $X_t \in R^{N\times 1}$ denotes $[x_{t,1}, x_{t,2}, \cdots, x_{t,N}]^T$ and is the state of all N nodes at time t, A is the state transition matrix and W_t represents noise with a Gaussian distribution:

$$W_t \sim \mathcal{N}(W_t|0, Q), \tag{2}$$

where Q is a positive definite covariance matrix which incorporates the randomness of the process and could be interpreted as physiological noise such as cardiac motion, blood flow, variation in respiratory volume etc. Similarly, the observation Y_t is a linear transformation of the state vector with added noise:

$$Y_t = HX_t + U_t, \tag{3}$$

where U_t is zero mean Gaussian noise and H is an identity matrix for direct observation. The matrix U_t captures measurement noise of the device, i.e. scanner noise, and adds another layer of robustness to the model.

Our aim is to learn A, the matrix of connectivity coefficients, where element $A_{i,j}$ represents a causal effect of node j on i. This feature of a directed network sets our approach apart from correlation-type methods, and offers an extended picture of the underlying functional networks in the brain. In addition, we seek to infer the unknown covariance matrix Q.

Employing a Gibbs sampler to iterate among the following set of conditional posterior distributions will result in convergence to the target distribution $\pi(A, Q, X_{1:T}|Y_{1:T})$:

$$\begin{gathered}\pi(X_{1:T}|A, Q, Y_{1:T}),\\ \pi(A|Q, X_{1:T}),\\ \pi(Q|A, X_{1:T}).\end{gathered}$$

It is straightforward to sample from the state conditional distribution $\pi(X_{1:T}|A, Q, Y_{1:T})$ using a Kalman filter followed by the application of backward sampling [48] [47]. To facilitate sampling of the covariance matrix, its distribution is formulated in terms of its inverse $\Upsilon = Q^{-1}$ and a conjugate

prior of a Wishart distribution is assumed on this precision matrix, such that:

$$\begin{aligned} p(\Upsilon) &= \mathcal{W}(\Upsilon|\nu,\Theta) \\ &\propto |\Upsilon|^{\nu/2}\exp\bigg(-\frac{1}{2}\mathrm{Tr}[\Theta^{-1}\Upsilon]\bigg), \end{aligned} \tag{4}$$

where the hyperparameters ν and Θ refer to the degrees of freedom and scale matrix respectively. Though it suffers from an inherent issue of dependence between variance and correlation [49], the Wishart distribution is chosen as its conjugacy feature results in convenient and efficient sampling, but could be easily replaced with another form of the conjugate prior in the Gibbs framework presented. For a non-conjugate prior, Metropolis-within-Gibbs could be employed.

Using this prior and the state conditional distribution, the conditional distribution of the precision matrix can be derived as:

$$\begin{aligned} \pi(\Upsilon|A,X_{1:T}) &= p(\Upsilon|A,X_{1:T},Y_{1:T}) \\ &\propto \pi(X_{1:T}|A,\Upsilon,Y_{1:T})p(\Upsilon) \\ &= \mathcal{W}(\Upsilon|\nu',\Theta'), \end{aligned} \tag{5}$$

where

$$\nu' = \nu + T - 1, \tag{6}$$

and

$$\Theta' = \bigg[\Theta^{-1} + \sum_{t=2}^{T}(X_t - AX_{t-1})(X_t - AX_{t-1})^T\bigg]^{-1}. \tag{7}$$

In order to include the feature of sparsity, each entry in the transition matrix is expressed as a product of a real number and a binary indicator. The transition matrix is then given by:

$$A = S \circ \Phi, \tag{8}$$

where $\Phi = [\phi_{i,j}]$, $S = [s_{i,j}]$, and $\circ$ represents the element-wise Hadamard product so that $A_{i,j} = [\phi_{i,j} \cdot s_{i,j}]$. The entries of S are indicator variables $s_{i,j} \in \{0,1\}$ which act as switches to allow elements of A to be turned on or off. The concept of sparsity has been previously employed in neuroimaging to analyse fMRI and EEG data using mainly regularisation schemes [50] [51] [52] [53] [54] [55]; here, the use of these indicator variables offers an alternative state-space approach to infer sparse representation. For each of these variables, an independent Bernoulli prior is assumed:

$$\begin{aligned} p(S) &= \prod_{i,j}\mathcal{BER}(s_{i,j}|\alpha) \\ &= \prod_{i,j}\alpha^{s_{i,j}}(1-\alpha)^{1-s_{i,j}}, \end{aligned} \tag{9}$$

where $\alpha \in [0,1]$ is a hyperparameter of the Bernoulli distribution and could be informed by structural connectivity from diffusion weighted imaging (DW-MRI). For the Φ set of variables, the conjugate prior is a multivariate normal distribution:

$$p(\Phi) = \mathcal{N}(a|m,P), \tag{10}$$

where $a = \mathrm{Vec}(A)$ is the vectorisation of the transition matrix, m is a zero vector and $P = vI$ is set to be a scaled identity matrix. It can be shown that if $X_{s,t}$ is defined by:

$$X_{s,t} = \begin{bmatrix} (X_t \circ \tilde{s}_1)^T & 0 & \cdots & 0 \\ 0 & (X_t \circ \tilde{s}_2)^T & \cdots & 0 \\ \vdots & \vdots & \ddots & \vdots \\ 0 & 0 & \cdots & (X_t \circ \tilde{s}_N)^T \end{bmatrix}, \tag{11}$$

such that $\tilde{s}_k^T$ is the k-th row of S and

$$\begin{aligned} AX_{t-1} &= (S \circ \Phi)X_{t-1} \\ &= X_{s,t-1}a, \end{aligned} \tag{12}$$

then the posterior conditional distribution of Φ is given as follows:

$$\begin{aligned} \pi(\Phi|S,\Upsilon,X_{1:T}) &= \pi(\Phi|S,\Upsilon,X_{1:T},Y_{1:T}) \\ &\propto p(X_{1:T}|\Phi,S,\Upsilon,Y_{1:T})p(\Phi) \\ &= \mathcal{N}(a|m',P'), \end{aligned} \tag{13}$$

where

$$P' = \bigg(P^{-1} + \sum_{t=2}^{T} X_{s,t-1}^T \Upsilon X_{s,t-1}\bigg)^{-1}, \tag{14}$$

and

$$m' = P'\bigg(P^{-1}m + \sum_{t=2}^{T} X_{s,t-1}^T \Upsilon X_t\bigg). \tag{15}$$

Sampling from $\pi(S|\Phi,\Upsilon,X_{1:T})$ to infer these indicator variables is difficult as the full joint distribution over all the elements of S is intractable. One way of sampling is to use individual conditional distributions $\pi(s_{i,j}|S_{-i,j},\Phi,\Upsilon,X_{1:T})$ in turn, where $S_{-i,j}$ refers to all elements of S except $s_{i,j}$. This is problematic because of the low probability of an element getting switched on from the off state. As the $\phi_{i,j}$ value is effectively sampled from the prior in Φ-sampling step when the corresponding $s_{i,j}$ is 0, its sampled value should fall in a region where $\pi(X_{1:T}|s_{i,j}=1,S_{-i,j},\Phi,\Upsilon)$ is large enough for $s_{i,j}=1$ to be drawn. This is very unlikely when using uninformative priors, and a solution to this issue is to draw samples $\{\phi_{i,j},s_{i,j}\}$ jointly from the appropriate conditional distribution using the following factorisation [56]:

$$\begin{aligned} &\pi(s_{i,j},\phi_{i,j}|S_{-i,j},\Phi_{-i,j},\Upsilon,X_{1:T}) \\ &\quad= \pi(s_{i,j}|S_{-i,j},\Phi_{-i,j},\Upsilon,X_{1:T}) \\ &\qquad\times \pi(\phi_{i,j}|S,\Phi_{-i,j},\Upsilon,X_{1:T}). \end{aligned} \tag{16}$$

This joint distribution is:

$$\begin{aligned} &\pi(s_{i,j},\phi_{i,j}|S_{-i,j},\Phi_{-i,j},\Upsilon,X_{1:T}) \\ &\quad= p(X_{1:T}|S,\Phi,\Upsilon)p(s_{i,j})p(\phi_{i,j}). \end{aligned} \tag{17}$$

If $\tilde{A}_{i,j}$ is defined as A with the (i,j)th entry replaced with 0, and $Z_{i,j}$ is a matrix of zeros with a single 1 in the (i,j)th location, then:

$$X_t - AX_{t-1} = (X_t - \tilde{A}_{i,j}X_{t-1}) - \phi_{i,j}s_{i,j}Z_{i,j}X_{t-1}, \quad (18)$$

This allows the state sequence probability to be written as:

$$\begin{aligned} &p(X_{1:T}|S,\Phi,\Upsilon) \\ &\propto \exp\Bigg(-\frac{1}{2}\Bigg[\phi_{i,j}^2 s_{i,j}^2 \sum_{t=2}^{T} X_{t-1}^T Z_{i,j}^T \Upsilon Z_{i,j} X_{t-1} \\ &\quad - 2\phi_{i,j}s_{i,j}\sum_{t=2}^{T} X_{t-1}^T Z_{i,j}^T \Upsilon (X_t - \tilde{A}_{i,j}X_{t-1})\Bigg]\Bigg), \end{aligned} \quad (19)$$

which is proportional with respect to $\phi_{i,j}$ and $s_{i,j}$. The joint distribution is therefore given by:

$$\begin{aligned} &\pi(s_{i,j},\phi_{i,j}|S_{-i,j},\Phi_{-i,j},\Upsilon,X_{1:T}) \propto \left(\alpha^{s_{i,j}}(1-\alpha)^{1-s_{i,j}}\right) \\ &\times \exp\Bigg(-\frac{1}{2}\Bigg[\phi_{i,j}^2\Bigg\{1/v + s_{i,j}^2\sum_{t=2}^{T} X_{t-1}^T Z_{i,j}^T \Upsilon Z_{i,j} X_{t-1}\Bigg\} \\ &- 2\phi_{i,j}\Bigg\{m_{i,j}/v + s_{i,j}\sum_{t=2}^{T} X_{t-1}^T Z_{i,j}^T \Upsilon (X_t - \tilde{A}_{i,j}X_{t-1})\Bigg\}\Bigg]\Bigg). \end{aligned} \quad (20)$$

By standard results of a Gaussian distribution, algebraic manipulation on this joint conditional posterior and marginalisation of $\phi_{i,j}$ leads to the following easy-to-sample Bernoulli distribution for the indicator variables:

$$\pi(s_{i,j}|S_{-i,j},\Phi_{-i,j},\Upsilon,X_{1:T}) \propto \kappa\lambda\left(\alpha^{s_{i,j}}(1-\alpha)^{1-s_{i,j}}\right), \quad (21)$$

where

$$\kappa = \left[1/v + s_{i,j}^2\sum_{t=2}^{T} X_{t-1}^T Z_{i,j}^T \Upsilon Z_{i,j} X_{t-1}\right]^{-1/2}, \quad (22)$$

and

$$\begin{aligned} &\lambda = \\ &\exp\left(\frac{1}{2}\frac{\left(\frac{m_{i,j}}{v} + s_{i,j}\sum_{t=2}^{T} X_{t-1}^T Z_{i,j}^T \Upsilon (X_t - \tilde{A}_{i,j}X_{t-1})\right)^2}{\frac{1}{v} + s_{i,j}^2\sum_{t=2}^{T} X_{t-1}^T Z_{i,j}^T \Upsilon Z_{i,j} X_{t-1}}\right). \end{aligned} \quad (23)$$

Conditioning the joint distribution on S, each of the parameters in the Φ set can be sampled from the following normal distribution:

$$\pi(\phi_{i,j}|S,\Phi_{-i,j},\Upsilon,X_{1:T}) = \mathcal{N}(\phi_{i,j}|m''_{i,j},v''_{i,j}), \quad (24)$$

where

$$v''_{i,j} = \frac{1}{v} + s_{i,j}^2\sum_{t=2}^{T} X_{t-1}^T Z_{i,j}^T \Upsilon Z_{i,j} X_{t-1}, \quad (25)$$

and

$$m''_{i,j} = v''_{i,j}\left(\frac{m_{i,j}}{v} + s_{i,j}\sum_{t=2}^{T} X_{t-1}^T Z_{i,j}^T \Upsilon (X_t - \tilde{A}_{i,j}X_{t-1})\right). \quad (26)$$

Thus, an efficient methodology due to joint sampling and the marginalisation of $\phi_{i,j}$ is formulated, which iteratively draws from the following full conditional distributions in order to estimate the unknown state system.

$\pi(X_{1:T}|S,\Phi,\Upsilon,Y_{1:T})$ by forward-filter backward-sampler,
$\pi(\Upsilon|\Phi,S,X_{1:T})$ by Equations 5-7,
$\pi(\Phi|S,\Upsilon,X_{1:T})$ by Equations 13-15,
$\pi(s_{i,j}|S_{-i,j},\Phi_{-i,j},\Upsilon,X_{1:T})$ by Equations 21-23,
$\pi(\phi_{i,j}|S,\Phi_{-i,j},\Upsilon,X_{1:T})$ by Equations 24-26.

III. Simulated Data

The algorithm is first tested on synthetic samples in order to verify its robustness and efficiency, and confirm its ability to yield meaningful results when applied to experimental fMRI data. This is demonstrated with a simulation example on a five dimensional model. The transition and covariance matrices are given by:

$$A = \begin{bmatrix} 0.9 & 0 & 0.2 & 0 & 0.1 \\ 0 & 0.8 & 0 & 0 & 0 \\ -0.1 & 0 & 0.9 & 0 & -0.1 \\ 0 & 0 & 0.3 & 0.7 & 0 \\ 0.2 & 0.5 & 0 & 0 & 0.8 \end{bmatrix},$$

and

$$Q = \begin{bmatrix} 0.55 & 0.38 & 0.42 & 0.39 & 0.39 \\ 0.38 & 0.45 & 0.41 & 0.46 & 0.42 \\ 0.42 & 0.41 & 0.55 & 0.49 & 0.39 \\ 0.39 & 0.46 & 0.49 & 0.52 & 0.46 \\ 0.39 & 0.42 & 0.39 & 0.46 & 0.50 \end{bmatrix}.$$

A time series with a length of 1650 points (to match the real data in the next section) is generated as shown in Figure 1. The parameters used are given in Table I, which set moderately vague priors, and the burn-in period N_{burn} is set to 10% of the total number of iterations $N_{samples}$. The results of the Gibbs sampler in terms of posterior histograms are displayed in Figures 2 and 3. Not only do the posterior distributions of the matrix elements match well with the true values, but so do the sparsity indicators in Figure 4, in which the cross elements of A are interpreted as the connectivity between different state variables while the elements of S as the probability that there exists a significant interaction between a pair of these variables.

In order to further examine the results, the convergence behaviour of the Markov chains is analysed. Figure 5 displays the sampled values for a few randomly selected elements of A and Q which shows fast convergence; the autocorrelation of the sampled values is consistently low which shows good mixing of the Markov chain, as demonstrated in the

Name	Description	Value
N	Number of nodes	5
T	Number of timesteps	1650
$N_{samples}$	Number of MCMC iterations	5000
N_{burn}	Burn-in period	500
ν	Degrees of freedom bound of Wishart prior	15
Θ	Scale matrix of Wishart prior	I
α	Hyperparameter of Bernoulli prior	0.5
v	Scale of covariance of multivariate Normal prior	100

TABLE I: List of parameters

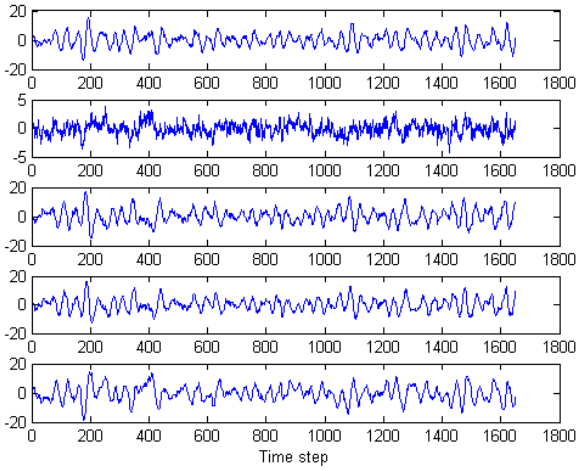

Fig. 1: Synthetic set of signals generated to test the algorithm.

autocorrelation function (ACF) plots of Figure 6.

It is difficult to benchmark the performance of simulated data results with those obtained from current methods such as correlation, as the realms of models and underlying assumptions are different, and any direct comparison of numerical errors obtained would not be a fair and accurate approach. For instance, generating signals from the model in Equation 1 and computing correlations would naturally result in numerical errors if compared to the results of the Gibbs scheme applied to the true model, and thus would be an unfair treatment. However, the validity of results acquired when applied to real data in the next section yields an insight into the employability of our proposed methodology, and paves avenues for its potential applicability in a clinical setting.

IV. Experimental Data

Twenty-two healthy subjects participated in a self-paced, right-handed finger opposition task-based, boxcar design experiment with five alternating cycles of task and fixation blocks. The participants had an age range of 19 to 57 with a mean of 35.0 and standard deviation of 11.2, and the male to female ratio was 13:9. The task comprised of touching one's fingers sequentially from index to little finger with the right thumb, and continuing to do so till the end of the task duration. This was followed by a rest period in which the participants were instructed to fixate on a crosshair in the middle of the screen. A visual *move* command was an indication to carry out the task, while *rest* was to stop it in order to enter the fixation state. Each cycle lasted for 30 seconds making the entire period of data acquisition for one participant to be five minutes.

fMRI data was obtained using a Siemens Trio 3T scanner with whole-brain echo planar imaging (TR = 2000 ms; TE = 30 ms; flip angle = 78°; FOV read = 192 mm; voxel size = 3.0 x 3.0 x 3.0 mm; volumes = 160; slices per volume= 32). Pre-processing of imaging data followed standard practices and involved standard slice-time and motion corrections, normalization to the Montreal Neurological Institute (MNI) space and an a-priori grey matter template, smoothing with an 8 mm FWHM Gaussian kernel, and low-pass filtering (0.009-0.08 Hz) [9] [57] [58] [59]. In addition, the time-series was de-trended by regressing out a linear term in order to remove residual signal drift [60]. The experiment was conducted at the Wolfson Brain Imaging Centre, Cambridge, UK and was approved by the local ethics committee with all participants having given informed consent in writing.

BOLD time-series data acquired for a total of ten regions corresponding to somatomotor [7] and visual cortices [61] was analysed. The names, drawn from the Automated Anatomical Labelling (AAL) atlas, and MNI co-ordinates of these regions of interest (ROIs) are listed in Table II. Spherical seeds of 6 mm radius were placed at these co-ordinates and the BOLD signals from all voxels within these regions were then averaged to obtain a representative signal for each node. Given the nature of the task, i.e. the engagement and disengagement of the motor control network in thirty seconds' cycles, it was hypothesised that the network formed by the motor ROIs would undergo a significant change in the two modes of activation and fixation, in contrast to that formed by the visual nodes.

To infer the Hadamard product in the connectivity matrix as well as the entire covariance matrix, the number of unknowns in a network of N nodes scale to $3N^2$. Though our Bayesian approach could be applied to individual data, with only 75 data points for each patient in either mode of activation or fixation in the experiment, it was not deemed appropriate to do so for inferring 300 parameters per person. Because of these temporal limitations of the data, fMRI measurements from the entire cohort were aggregated to form one large time series and our algorithm was applied separately to the active and fixated states for each network. The distributional measure obtained becomes relevant here as the shape of the posterior distribution retains information about the variability among subjects, as opposed to a point estimate in which all such information is lost. The same parameter values as those in the previous section are used except for ν, which is increased by two orders of magnitude to restrict the prior for covariance to small values. Without doing so, the matrix A is not inferred as all connectivity is captured in the noise matrix Q.

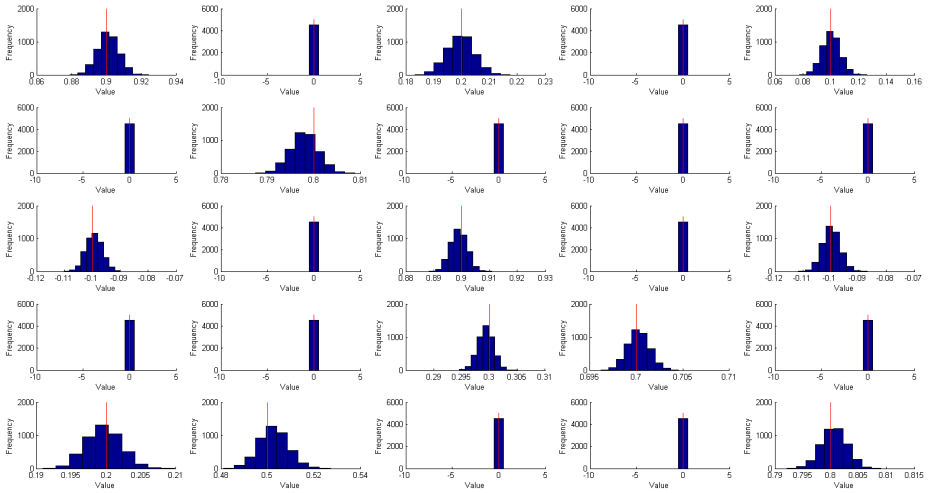

Fig. 2: Posterior histograms for the simulated transition matrix A. Vertical lines indicate true values for the synthetic data.

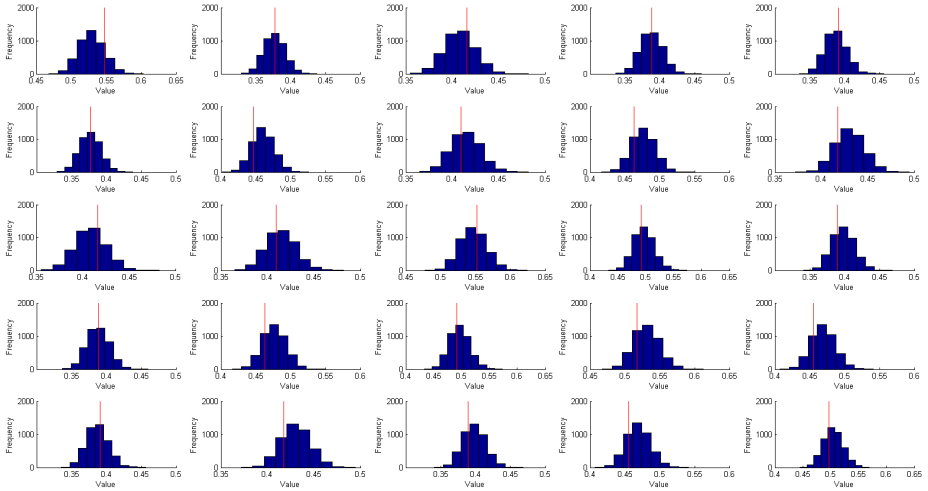

Fig. 3: Posterior histograms for the simulated covariance matrix Q. Vertical lines indicate true values for the synthetic data.

ROI	Name	Abbreviation	Co-ordinates
Motor	Supplementary Motor Area	SMA	[-4 -2 54]
	Left Pre-central Gyrus	$PRECG_L$	[-36 -22 64]
	Right Pre-central Gyrus	$PRECG_R$	[60 8 28]
	Left Post-central Gyrus	$POCG_L$	[-40 -26 52]
	Right Post-central Gyrus	$POCG_R$	[56 -16 38]
Visual	Left Lingual Gyrus	$LING_L$	[-15 -72 -8]
	Right Lingual Gyrus	$LING_R$	[18 -47 -10]
	Left Calcarine	$LCAL_L$	[-18 -68 5]
	Right Calcarine	$LCAL_R$	[8 -72 -8]
	Right Fusiform Gyrus	FFG_R	[27 -59 -9]

TABLE II: Details of regions of interest (ROIs) corresponding to motor and visual functions

Figure 7 shows the posterior distributions for the connectivity matrix A of the motor nodes while Figure 8 shows the same for the visual network. On average, the motor network is more strongly connected in the active state which shows at least eight connections that disappear in the fixated state. Because of the use of right hand in

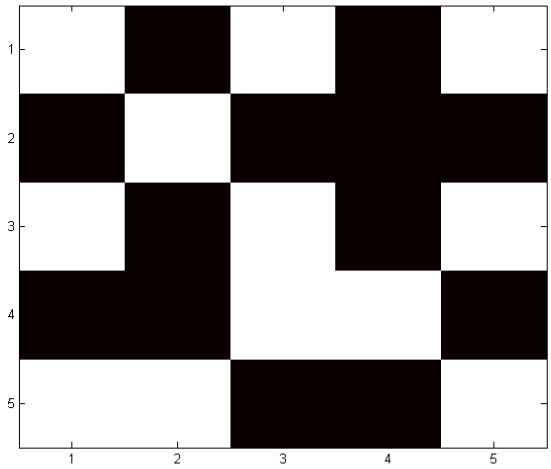

Fig. 4: Strucuture of connectivity matrix through inference of sparsity indicators. The bright (white) positions indicate non-zero values in the structure of A while the dark locations correspond to zeros.

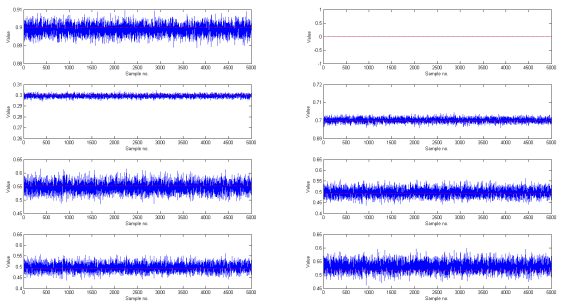

Fig. 5: Markov chains plotted for randomly selected elements of A and Q.

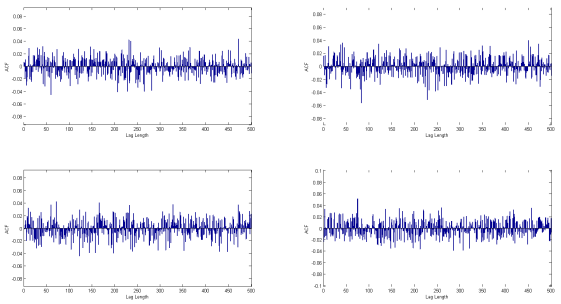

Fig. 6: Autocorrelation function (ACF) plots for some elements of A and Q.

the experiment, significant activity is observed in the left hemisphere with both the pre and post central hemisphere displaying connectivity not only between themselves but also with supplementary motor area and the right hemisphere. In the fixated state, it is interesting to note that both nodes from the left hemisphere appear to be anticorrelated with the supplementary motor area, an observation which matches with those found in exisiting literature [2] [62].

On the other hand, the visual network also exhibits some changes. A total of five connections, three of which display anticorrelation, are seen in the active state which disappear in the fixated state. However, five new connections appear in the fixated state in which the right lingual hemisphere is more connected to all other nodes. The variation could be explained by the fact that the participants may be visually engaged in a different manner during the fixated state as they searched for visual cues to restart the motor task. In short, despite the observed changes in connectivity, the visual network does not favourably connect more in either the active or fixation state, unlike its motor counterpart. Thus, these findings have sufficiently matched our initial hypothesis and have helped in subtantiating the validity of our work and laying the foundation for further analysis.

In addition, the shapes of the displayed histograms provide information about the variability component among subjects. For both types of network, the fixated state generally has broader spectrums for active connections e.g. $A_{(2,3)}$, $A_{(4,1)}$ for motor, and $A_{(4,1)}$, $A_{(4,5)}$ for the visual network. This could be interpreted as participants having varied levels of activity while executing the task but exhibiting similar states of rest in the fixation mode.

V. Conclusion

By examining a real life case with a clear hypothesis in which the motor network changed more significantly than the visual network, we have demonstrated the use of a linear Bayesian model to infer functional connectivity along with causal information, where Gibbs sampling was used to approximate posterior distributions.

One of the main drawbacks of such a sampling method is the computational cost associated with it. The complexity of the overall sampling of Φ is $O(N^6)$ [63] which could be reduced to $O(N^4)$ [64]; however, the complexity of the complete framework presented is dominated by the element-wise sampling step, which being $O(N^4T)$ is higher than that of point-based conventional methods (i.e. $O(N^2T)$). But what limits the scalability of the current approach, as is the case in DCM, is not its speed but the problems associated with convergence to the true values in a large parameter space. Thus, the extension of our proposed methodology to networks of larger sizes, for instance through paradigms of dimensionality reduction and blocked sampling [65] [66] [67] [68], could be taken as direction for future work.

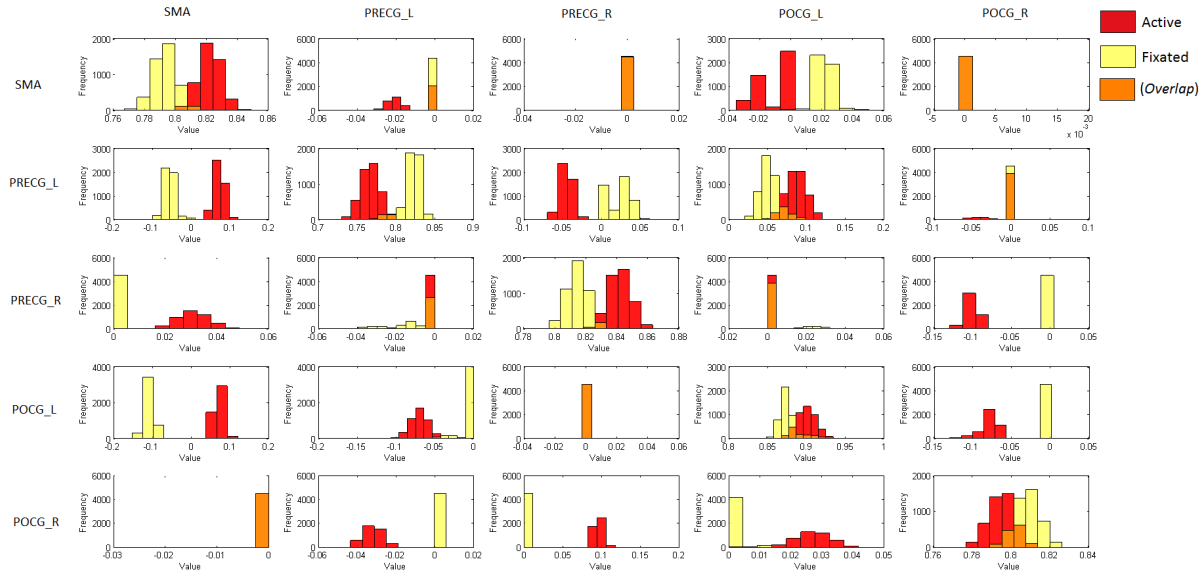

Fig. 7: Posterior histograms of the connectivity matrix elements for the motor network. The red bars show the distribution in the active state, the yellow bars in the fixated state, and the orange bars represent the overlap of the two distributions.

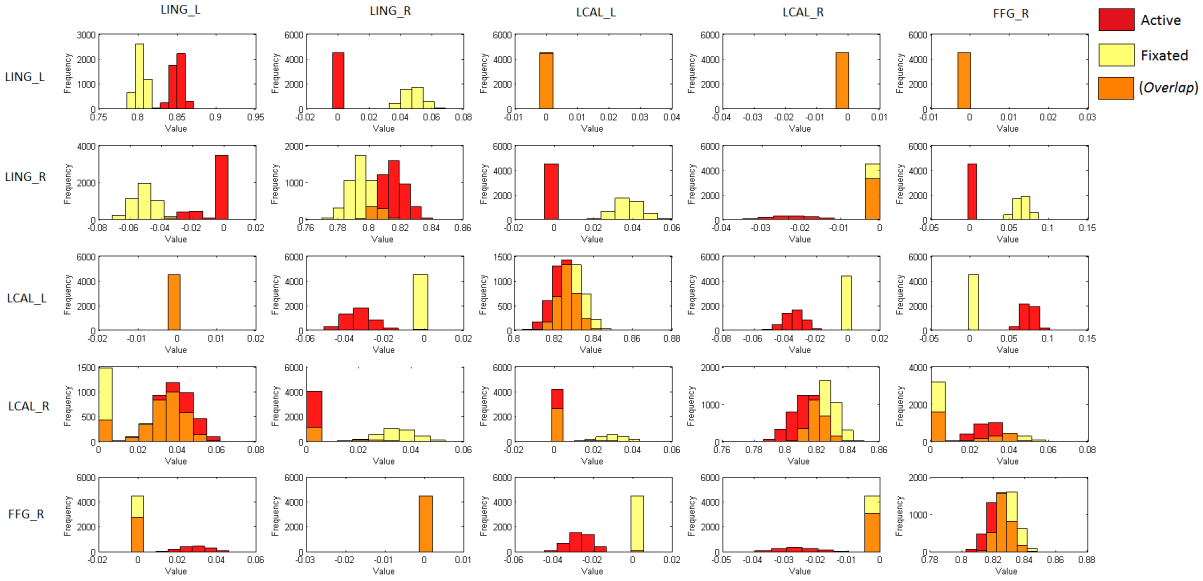

Fig. 8: Posterior histograms of the connectivity matrix elementss for the visual network. The red bars show the distribution in the active state, the yellow bars in the fixated state, and the orange bars represent the overlap of the two distributions.

The issue of high sensitivity to the innate parameter of the state precision matrix Υ could be explored further - one possibility is to fix this matrix (e.g. to a scaled identity) to capture all structure in A and to infer the observation noise matrix U instead, using concepts presented in [69]. In addition, experiments could be redesigned to allow for collection of more data from each subject so that the algorithm could be applied at the individual-level without the need to concatenate. This would provide information about both the group-level as well as subject-level variance components.

Recent research has suggested that dynamic functional connectivity exhibited by BOLD signals in resting-state may have clinical value [70] [71] [72] [73] [74]. Having validated the proposed methodology and demonstrated its potential use, the unknown realms of resting-state data could be delved into for attempting inference of parameters that smoothly vary with time. This more complicated case could be implemented through the use of Sequential Monte Carlo [75] [76] and Particle MCMC methods [77], and could yield an even more comprehensive understanding of brain functions. In order to gain a better insight into the underlying neuronal states and obtain more biologically relevant information, the work could be further expanded to examine dynamic effective

connectivity through the use of non-linear observation models, such as the Balloon model for haemodynamic response [78] [79] [80] [81] [82].

Moreover, studies could be conducted on healthy controls and patients in order to explore the implications of our work in a clinical context. For example, based on the evidence that suggests changes in functional and structural connectivity following traumatic brain injury [20] [21] [83] [84] [85], a comparison could be made between healthy participants and traumatic brain injury patients under drug-free and drug-induced conditions.

ACKNOWLEDGMENT

This work was supported by the Engineering and Physical Sciences Research Council (EPSRC) grant number EP/K020153/1 and Yousef Jameel Scholarship Programme.

REFERENCES

[1] M. Cole, D. Bassett, J. Power, T. Braver, and S. Petersen, "Intrinsic and Task-Evoked Network Architectures of the Human Brain," *Neuron*, vol. 83, no. 1, pp. 238–251, 2014.

[2] M. D. Fox, A. Z. Snyder, J. L. Vincent, M. Corbetta, D. C. Van Essen, and M. E. Raichle, "The human brain is intrinsically organized into dynamic, anticorrelated functional networks," *PNAS*, vol. 102, no. 27, pp. 9673–8, 2005.

[3] D. A. Leopold and A. Maier, "Ongoing physiological processes in the cerebral cortex," *NeuroImage*, vol. 62, no. 4, pp. 2190–2200, 2012.

[4] R. Patriat, E. K. Molloy, T. B. Meier, G. R. Kirk, V. A. Nair, M. E. Meyerand, V. Prabhakaran, and R. M. Birn, "The effect of resting condition on resting-state fMRI reliability and consistency: A comparison between resting with eyes open, closed, and fixated," *NeuroImage*, vol. 78, pp. 463–473, 2013.

[5] S. M. Smith, P. T. Fox, K. L. Miller, D. C. Glahn, P. M. Fox, C. E. Mackay, N. Filippini, K. E. Watkins, R. Toro, A. R. Laird, and C. F. Beckmann, "Correspondence of the brain's functional architecture during activation and rest," *PNAS*, vol. 106, no. 31, pp. 13040–13045, 2009.

[6] A. R. Laird, P. M. Fox, S. B. Eickhoff, J. A. Turner, K. L. Ray, D. R. McKay, D. C. Glahn, C. F. Beckmann, S. M. Smith, and P. T. Fox, "Behavioral interpretations of intrinsic connectivity networks," *Journal of cognitive neuroscience*, vol. 23, pp. 4022–37, dec 2011.

[7] D. Vatansever, D. Menon, A. Manktelow, B. Sahakian, and E. Stamatakis, "Default mode network connectivity during task execution," *NeuroImage*, vol. 122, pp. 96–104, 2015.

[8] J. S. Damoiseaux and M. D. Greicius, "Greater than the sum of its parts: a review of studies combining structural connectivity and resting-state functional connectivity," *Brain Structure and Function*, vol. 213, no. 6, pp. 525–533, 2009.

[9] D. Vatansever, D. K. Menon, A. E. Manktelow, B. J. Sahakian, and E. A. Stamatakis, "Default Mode Dynamics for Global Functional Integration," *The Journal of neuroscience*, vol. 35, no. 46, pp. 15254–15262, 2015.

[10] E. Bullmore and O. Sporns, "Complex brain networks: graph theoretical analysis of structural and functional systems," *Nature reviews. Neuroscience*, vol. 10, pp. 186–98, mar 2009.

[11] S. M. Smith, K. L. Miller, S. Moeller, J. Xu, E. J. Auerbach, M. W. Woolrich, C. F. Beckmann, M. Jenkinson, J. Andersson, M. F. Glasser, D. C. Van Essen, D. A. Feinberg, E. S. Yacoub, and K. Ugurbil, "Temporally-independent functional modes of spontaneous brain activity," *PNAS*, vol. 109, pp. 3131–6, feb 2012.

[12] A. Fornito and E. T. Bullmore, "Connectomics: A new paradigm for understanding brain disease," *European neuropsychopharmacology: the journal of the European College of Neuropsychopharmacology*, mar 2014.

[13] O. Sporns, "The human connectome: a complex network," *Annals of the New York Academy of Sciences*, vol. 1224, pp. 109–25, apr 2011.

[14] C. F. Beckmann, M. DeLuca, J. T. Devlin, and S. M. Smith, "Investigations into resting-state connectivity using independent component analysis," *Philosophical transactions of the Royal Society of London. Series B, Biological sciences*, vol. 360, no. 1457, pp. 1001–1013, 2005.

[15] J. S. Damoiseaux, S. A. R. B. Rombouts, F. Barkhof, P. Scheltens, C. J. Stam, S. M. Smith, and C. F. Beckmann, "Consistent resting-state networks," *PNAS*, vol. 103, no. 37, 2006.

[16] C. F. Beckmann, "Modelling with independent components," *NeuroImage*, vol. 62, pp. 891–901, aug 2012.

[17] D. T. Jones, P. Vemuri, M. C. Murphy, J. L. Gunter, M. L. Senjem, M. M. Machulda, S. A. Przybelski, B. E. Gregg, K. Kantarci, D. S. Knopman, B. F. Boeve, R. C. Petersen, and C. R. Jack, "Non-stationarity in the "resting brain's" modular architecture," *PLoS ONE*, vol. 7, no. 6, 2012.

[18] S. Whitfield-Gabriel, H. Thermenos, S. Milanovic, and M. T. Tsuang, "Hyperactivity and hyperconnectivity of the default network in schizophrenia and in first-degree relatives of persons with schizophrenia," *PNAS*, vol. 106, no. 4, pp. 1279–1284, 2009.

[19] M. Kasahara, D. K. Menon, C. H. Salmond, J. G. Outtrim, J. V. Taylor Tavares, T. A. Carpenter, J. D. Pickard, B. J. Sahakian, and E. A. Stamatakis, "Altered functional connectivity in the motor network after traumatic brain injury," *Neurology*, vol. 75, pp. 168–76, jul 2010.

[20] M. Kasahara, D. K. Menon, C. H. Salmond, J. G. Outtrim, J. V. T. Tavares, T. A. Carpenter, J. D. Pickard, B. J. Sahakian, and E. A. Stamatakis, "Traumatic brain injury alters the functional brain network mediating working memory," *Brain Injury*, vol. 25, no. 12, pp. 1170–1187, 2011.

[21] V. Bonnelle, R. Leech, K. M. Kinnunen, T. E. Ham, C. F. Beckmann, X. De Boissezon, R. J. Greenwood, and D. J. Sharp, "Default Mode Network Connectivity Predicts Sustained Attention Deficits after Traumatic Brain Injury," *Journal of Neuroscience*, vol. 31, no. 38, pp. 13442–13451, 2011.

[22] J. Damoiseaux, C. Beckmann, E. S. Arigita, F. Barkhof, P. Scheltens, C. Stam, S. Smith, and S. Rombouts, "Reduced resting-state brain activity in the default network in normal aging," *Cerebral Cortex*, vol. 18, no. 8, pp. 1856–1864, 2008.

[23] E. A. Stamatakis, R. M. Adapa, A. R. Absalom, and D. K. Menon, "Changes in Resting Neural Connectivity during Propofol Sedation," *PLoS ONE*, vol. 5, no. 12, 2010.

[24] K. J. Friston, "Functional and effective connectivity: a review," *Brain connectivity*, vol. 1, pp. 13–36, jan 2011.

[25] K. Friston, L. Harrison, and W. Penny, "Dynamic causal modelling," *NeuroImage*, vol. 19, pp. 1273–1302, aug 2003.

[26] K. J. Friston, B. Li, J. Daunizeau, and K. E. Stephan, "Network discovery with DCM," *NeuroImage*, vol. 56, pp. 1202–21, jun 2011.

[27] B. Li, J. Daunizeau, K. E. Stephan, W. Penny, D. Hu, and K. Friston, "Generalised filtering and stochastic DCM for fMRI," *NeuroImage*, vol. 58, pp. 442–57, oct 2011.

[28] A. R. Mclntosh, "Structural Equation Modeling and Its Application to Network Analysis in Functional Brain Imaging," *Human Brain Mapping*, vol. 22, pp. 2–22, 1994.

[29] W. D. Penny, K. E. Stephan, A. Mechelli, and K. J. Friston, "Modelling functional integration: A comparison of structural equation and dynamic causal models," *NeuroImage*, vol. 23, pp. 264–274, 2004.

[30] G. Deshpande, S. LaConte, G. A. James, S. Peltier, and X. Hu, "Multivariate granger causality analysis of fMRI data," *Human Brain Mapping*, vol. 30, no. 4, pp. 1361–1373, 2009.

[31] A. K. Seth, A. B. Barrett, and L. Barnett, "Granger Causality Analysis in Neuroscience and Neuroimaging," *Journal of Neuroscience*, vol. 35, no. 8, pp. 3293–3297, 2015.

[32] D. Marinazzo, W. Liao, H. Chen, and S. Stramaglia, "Nonlinear connectivity by Granger causality," *NeuroImage*, vol. 58, no. 2, pp. 330–338, 2011.

[33] M. M. Monti, "Statistical Analysis of fMRI Time-Series: A Critical Review of the GLM Approach," *Frontiers in Human Neuroscience*, vol. 5, no. 609, p. 28, 2011.

[34] C. F. Beckmann, M. Jenkinson, and S. M. Smith, "General multilevel linear modeling for group analysis in fMRI," *NeuroImage*, vol. 20, no. 2, pp. 1052–1063, 2003.

[35] M. W. Woolrich, T. E. J. Behrens, C. F. Beckmann, M. Jenkinson, and S. M. Smith, "Multilevel linear modelling for fMRI group analysis using Bayesian inference," *NeuroImage*, vol. 21, pp. 1732–47, apr 2004.

[36] K. J. Friston, N. Trujillo-Barreto, and J. Daunizeau, "DEM: a variational treatment of dynamic systems," *NeuroImage*, vol. 41, pp. 849–85, jul 2008.

[37] J. Daunizeau, K. J. Friston, and S. J. Kiebel, "Variational Bayesian identification and prediction of stochastic nonlinear dynamic causal models," *Physica D.*, vol. 238, pp. 2089–2118, nov 2009.

[38] D. Jacobsen, K. Madsen, and L. Hansen, "Identification of Non-Linear Models of Neural Activity in BOLD fMRI," *ISBI*, pp. 952–955, 2006.

[39] L. A. Johnston, E. Duff, I. Mareels, and G. F. Egan, "Nonlinear estimation of the BOLD signal," *NeuroImage*, vol. 40, pp. 504–14, apr 2008.

[40] G. Marrelec, A. Krainik, H. Duffau, J. Doyon, and H. Benali, "Partial correlation for functional brain interactivity investigation in functional MRI," *NeuroImage*, vol. 32, no. 1, pp. 228–237, 2006.

[41] J. Kang, L. Wang, C. Yan, J. Wang, X. Liang, and Y. He, "Characterizing dynamic functional connectivity in the resting brain using variable parameter regression and Kalman filtering approaches," *NeuroImage*, vol. 56, no. 3, pp. 1222–1234, 2011.

[42] M. Hinne, L. Ambrogioni, R. J. Janssen, T. Heskes, and M. A. J. van Gerven, "Structurally-informed Bayesian functional connectivity analysis," *NeuroImage*, vol. 86, pp. 294–305, 2014.

[43] M. Hinne, R. J. Janssen, T. Heskes, and M. A. J. van Gerven, "Bayesian Estimation of Conditional Independence Graphs Improves Functional Connectivity Estimates," *PLoS Computational Biology*, vol. 11, no. 11, pp. 1–26, 2015.

[44] J. L. Vincent, "Learning and Memory: While You Rest, Your Brain Keeps Working," *Current Biology*, vol. 19, no. 12, pp. 484–486, 2009.

[45] L. Kuo and B. Mallick, "Variable Selection for Regression Models," *Sankhya:The Indian Journal of Statistics, Series B (1962-2002)*, vol. 60, no. 1, pp. 65–81, 1998.

[46] M. Zhou, H. Chen, and L. Ren, "Non-parametric Bayesian dictionary learning for sparse image representations," *Advances in Neural Information Processing Systems*, pp. 2295–2303, 2009.

[47] A. Wills, T. Schön, F. Lindsten, and B. Ninness, "Estimation of Linear Systems using a Gibbs Sampler," *System Identification*, pp. 2–7, 2012.

[48] C. K. Carter and R. Kohn, "On Gibbs Sampling for State Space Models," *Biometrika* vol. 81, no. 3, pp. 541–553, 1994.

[49] I. Alvarez, J. Niemi, and M. Simpson, "Bayesian Inference for a Covariance Matrix," *Annual Conference Proceedings on Applied Statistics in Agriculture*, pp. 71–82, 2004.

[50] G. Flandin and W. D. Penny, "Bayesian fMRI data analysis with sparse spatial basis function priors," *NeuroImage*, vol. 34, no. 3, pp. 1108–1125, 2007.

[51] S. Ryali, T. Chen, K. Supekar, and V. Menon, "Estimation of functional connectivity in fMRI data using stability selection-based sparse partial correlation with elastic net penalty," *NeuroImage*, vol. 59, no. 4, pp. 3852–3861, 2012.

[52] S. Ryali, K. Supekar, D. A. Abrams, and V. Menon, "Sparse logistic regression for whole-brain classification of fMRI data," *NeuroImage*, vol. 51, no. 2, pp. 752–764, 2010.

[53] L. Ding, Y. Ni, J. Sweeney, and B. He, "Sparse cortical current density imaging in motor potentials induced by finger movement," *Journal of Neural Engineering*, vol. 8, no. 3, p. 036008, 2011.

[54] L. Ding and B. He, "Sparse Source Imaging in EEG with Accurate Field Modeling," *Human Brain Mapping*, vol. 29, no. 9, pp. 1053–1067, 2008.

[55] P. Valdes-Sosa, J. Sanchez-Bornot, and A. Lage-Castellanos, "Estimating brain functional connectivity with sparse multivariate autoregression," *Phil. Trans. R. Soc.*, vol. 360, pp. 969–981, 2005.

[56] P. J. Wolfe, S. J. Godsill, and W. J. Ng, "Bayesian variable selection and regularization for timefrequency surface estimation," *Journal of the Royal Statistical Society: Series B (Statistical Methodology)*, vol. 66, no. 3, pp. 575–589, 2004.

[57] M. Allen, J. Smallwood, J. Christensen, D. Gramm, B. Rasmussen, C. G. Jensen, A. Roepstorff, and A. Lutz, "The balanced mind: the variability of task-unrelated thoughts predicts error monitoring," *Frontiers in Human Neuroscience*, vol. 7, 2013.

[58] A. Boghi, R. Rasetti, F. Avidano, C. Manzone, L. Orsi, F. D'Agata, P. Caroppo, M. Bergui, P. Rocca, L. Pulvirenti, G. B. Bradac, F. Bogetto, R. Mutani, and P. Mortara, "The effect of gender on planning: An fMRI study using the Tower of London task," *NeuroImage*, vol. 33, no. 3, pp. 999–1010, 2006.

[59] R. Salomon, D. R. Levy, and R. Malach, "Deconstructing the default: Cortical subdivision of the default mode/intrinsic system during self-related processing," *Human Brain Mapping*, vol. 35, no. 4, pp. 1491–1502, 2014.

[60] K Murphy, R. M. Birn, D. A. Handwerker, T. B. Jones, and P. A. Bandettini, "The impact of global signal regression on resting state correlations: Are anti-correlated networks introduced?," *NeuroImage*, vol. 44, no. 3, pp. 893–905, 2009.

[61] K. Wang, T. Jiang, C. Yu, L. Tian, J. Li, Y. Liu, Y. Zhou, L. Xu, M. Song, and K. Li, "Spontaneous activity associated with primary visual cortex: a resting-state fMRI study," *Cerebral Cortex*, vol. 18, no. 3, pp. 697–704, 2008.

[62] M. D. Fox, D. Zhang, A. Z. Snyder, and M. E. Raichle, "The global signal and observed anticorrelated resting state brain networks," *Journal of Neurophysiology*, vol. 101, no. 6, pp. 3270–83, 2009.

[63] J. Hartikainen and S. Särkkä, "Kalman filtering and smoothing solutions to temporal Gaussian process regression models," *Proceedings of the 2010 IEEE International Workshop on Machine Learning for Signal Processing*, pp. 379–384, 2010.

[64] J. Murphy and S. Godsill, "Efficient Filtering and Sampling for a Class of Time Varying Linear Systems," *IEEE Transactions on International Conference on Acoustics, Speech and Signal Processing* no. 2, pp. 3701–3705, 2015.

[65] D. Venugopal and V. Gogate, "Dynamic blocking and collapsing for gibbs sampling," *Proceedings of the Twenty-Ninth Conference on Uncertainty in Artificial Intelligence*, 2013.

[66] S. J. Kiebel, O. David, and K. J. Friston, "Dynamic causal modelling of evoked responses in EEG/MEG with lead field parameterization," *NeuroImage*, vol. 30, no. 4, pp. 1273–1284, 2006.

[67] A. Doucet, M. Briers, and S. Sénécal, "Efficient Block Sampling Strategies for Sequential Monte Carlo Methods," *Journal of Computational and Graphical Statistics*, vol. 15, no. 3, pp. 693–711, 2006.

[68] M. L. Seghier and K. J. Friston, "Network discovery with large DCMs," *NeuroImage*, vol. 68, pp. 181–91, mar 2013.

[69] M. J. Beal and Z. Ghahramani, "Variational Bayesian Learning of Directed Graphical Models with Hidden Variables," *Bayesian Analysis*, vol. 1, no. 4, pp. 793–832, 2006.

[70] R. M. Hutchison, T. Womelsdorf, E. A. Allen, P. A. Bandettini, V. D. Calhoun, M. Corbetta, S. Della Penna, J. H. Duyn, G. H. Glover, J. Gonzalez-Castillo, D. A. Handwerker, S. Keilholz, V. Kiviniemi, D. A. Leopold, F. de Pasquale, O. Sporns, M. Walter, and C. Chang, "Dynamic functional connectivity: promise, issues, and interpretations," *NeuroImage*, vol. 80, pp. 360–78, oct 2013.

[71] R. M. Hutchison, T. Womelsdorf, J. S. Gati, S. Everling, and R. S. Menon, "Resting-state networks show dynamic functional connectivity in awake humans and anesthetized macaques," *Human Brain Mapping*, vol. 34, pp. 2154–77, sep 2013.

[72] U. Sakoglu, G. D. Pearlson, K. A. Kiehl, Y. M. Wang, A. M. Michael, and V. D. Calhoun, "A method for evaluating dynamic functional network connectivity and task-modulation: application to schizophrenia," *Magn Reson Mater Phy*, vol. 23, pp. 351–66, dec 2010.

[73] D. A. Handwerker, V. Roopchansingh, J. Gonzalez-Castillo, and P. A. Bandettini, "Periodic changes in fMRI connectivity," *NeuroImage*, vol. 63, pp. 1712–9, nov 2012.

[74] E. A. Allen, E. Damaraju, S. M. Plis, E. B. Erhardt, T. Eichele, and V. D. Calhoun, "Tracking whole-brain connectivity dynamics in the resting state," *Cerebral Cortex*, vol. 24, pp. 663–676, mar 2014.

[75] O. Cappe, S. J. Godsill, and E. Moulines, "An Overview of Existing Methods and Recent Advances in Sequential Monte Carlo," *Proceedings of the IEEE*, vol. 95, pp. 899–924, may 2007.

[76] S. K. Pang, J. Li, and S. J. Godsill, "Detection and Tracking of Coordinated Groups," *IEEE Transactions on Aerospace and Electronic Systems*, vol. 47, pp. 472–502, jan 2011.

[77] C. Andrieu, A. Doucet, and R. Holenstein, "Particle Markov chain Monte Carlo methods," *Journal of the Royal Statistical Society: Series B (Statistical Methodology)*, vol. 72, pp. 269–342, jun 2010.

[78] K. J. Friston, A. Mechelli, R. Turner, and C. J. Price, "Nonlinear responses in fMRI: the Balloon model, Volterra kernels, and other hemodynamics," *NeuroImage*, vol. 12, pp. 466–77, oct 2000.

[79] K. E. Stephan, N. Weiskopf, P. M. Drysdale, P. A. Robinson, and K. J. Friston, "Comparing hemodynamic models with DCM," *NeuroImage*, vol. 38, pp. 387–401, nov 2007.

[80] R. B. Buxton, K. Uluda, D. J. Dubowitz, and T. T. Liu, "Modeling the hemodynamic response to brain activation," *NeuroImage*, vol. 23 Suppl 1, pp. S220–33, jan 2004.

[81] Z. Hu, X. Zhao, H. Liu, and P. Shi, "Nonlinear Analysis of the BOLD Signal," *EURASIP Journal on Advances in Signal Processing*, vol. 2009, no. 1, p. 215409, 2009.

[82] K. E. Stephan, L. Kasper, L. M. Harrison, J. Daunizeau, H. E. M. den Ouden, M. Breakspear, and K. J. Friston, "Nonlinear dynamic causal models for fMRI," *NeuroImage*, vol. 42, pp. 649–62, aug 2008.

[83] D. J. Sharp, C. F. Beckmann, R. Greenwood, K. M. Kinnunen, V. Bonnelle, X. De Boissezon, J. H. Powell, S. J. Counsell, M. C. Patel, and R. Leech, "Default mode network functional and structural connectivity

after traumatic brain injury," *Brain*, vol. 134, no. 8, pp. 2233–2247, 2011.

[84] V. Bonnelle, T. Ham, R. Leech, K. Kinnunen, M. Mehta, R. Greenwood, and D. Sharp, "Salience network integrity predicts default mode network function after traumatic brain injury," vol. 109, no. 12, pp. 4690–4695, 2012.

[85] D. J. Sharp, G. Scott, and R. Leech, "Network dysfunction after traumatic brain injury," *Nature reviews. Neurology*, vol. 10, no. 3, pp. 156–66, 2014.

M. Faizan Ahmad received the M.Eng. degree in Engineering Science from Oxford University, U.K. in 2012. He is currently pursuing the Ph.D. degree in the Signal Processing Group, Engineering Department, Cambridge University, U.K. His research interests include Sequential Monte Carlo and Markov Chain Monte Carlo methods for inference of brain connectivity using functional Magnetic Resonance Imaging (fMRI).

James Murphy received the undergraduate degree from Cambridge University, U.K., the M.Sc. degree in Mathematical Modelling from Oxford University, U.K., and the Ph.D. degree in the Signal Processing Group, Engineering Department, Cambridge University, U.K. Before this, he worked as a Senior Analyst with a quantitative finance consulting firm. His research interests include Monte Carlo methods for inference in univariate and multivariate time series problems.

Deniz Vatansever received the B.Sc. degree in Neuroscience from Trinity College, U.S.A., the M.Sc. degree in Integrative Neurosciences from Imperial College London, U.K., and the Ph.D. degree in Clinical Neurosciences from Cambridge University, U.K. He is currently a Research Associate at the Department of Psychology, York University, U.K. His research interests include network analysis and graph theory for human cognition using fMRI.

Emmanuel A Stamatakis leads the Functional Imaging Group at the Division of Anaesthesia, School of Clinical Medicine, Cambridge University, U.K. He is also the Stephen Erskine Fellow at Queens College, Cambridge, U.K. His current research interests are in functional and structural connectivity analyses, for task and resting state functional Magnetic Resonance Imaging, as means to investigating organisation and reorganisation/plasticity in the human brain.

Simon J Godsill is the Professor of Statistical Signal Processing in the Engineering Department of Cambridge University, U.K. He has research interests in Bayesian and statistical methods for signal processing, Monte Carlo algorithms for Bayesian problems, modelling and enhancement of audio and musical signals, tracking, and high-frequency financial data. He has published extensively in journals, books and conferences. Prof. Godsill has acted as an Associate Editor for the IEEE Transactions on Signal Processing and the Journal Bayesian Analysis, and as a member of IEEE Signal Processing Theory and Methods Committee. He has coedited in 2002 a special issue of the IEEE Transactions on Signal Processing on Monte Carlo Methods in Signal Processing, and has organised many conference sessions on related themes.